J. Fluid Mech. (2004), *vol.* 504, *pp.* 365–389.
DOI: 10.1017/S0022112004008262 Printed in the United Kingdom

Some investigations on the use of ultrasonics in travelling bubble cavitation control

By DHIMAN CHATTERJEE AND VIJAY H. ARAKERI

Department of Mechanical Engineering, Indian Institute of Science, Bangalore 560 012, India

(Received 1 November 2002 and in revised form 6 August 2003)

In this paper we report results from some investigations on the use of ultrasonics in controlling travelling bubble cavitation. Control of this type of cavitation, generated using a venturi device, has been achieved by manipulation of potential nuclei using a piezoelectric device, termed the *Ultrasonic Nuclei Manipulator* (UNM). The performance of the UNM, activated in continuous-wave (CW) and pulsed modes, has been studied over a range of dissolved gas concentration (C). The performance under CW-excitation is found to depend sensitively on C, with lack of control in near-saturated water samples. Failure to control cavitation at $C \approx 1$ under CW-excitation is suggested to be a result of bubble growth by rectified diffusion under these conditions. The pulsed mode of excitation of the UNM, in such cases, seems to be a very promising alternative. Further improvement is observed by using two piezoelectric crystals, one driven in the CW-mode and the second in pulsed mode, as the UNM. Through carefully designed experimentation, this has been traced to the movement of nuclei under the influence of Bjerknes forces. Besides reduction of noise, other measures of control have been identified and investigated. For example, it has been found that the maximum velocity achievable at the venturi throat can be increased from about $15\,\mathrm{m\,s^{-1}}$ to about $22\,\mathrm{m\,s^{-1}}$ with nuclei manipulation using ultrasonics.

1. Introduction

Cavitation refers to the formation and subsequent dynamic life of bubbles in liquids subjected to a sufficiently low pressure. These bubbles can be either gas or vapour filled and can occur in a variety of liquids under a wide range of operating conditions. The required low pressure can be created either by an imposed acoustic field produced by a piezoelectric crystal or due to the flow of liquid through a constricted passage as in a venturi throat. Depending upon its origin, cavitation can be termed as acoustic or hydrodynamic.

Central to the understanding of acoustic cavitation is the interaction of a bubble with an imposed acoustic field. Depending on the driving frequency and the pressure amplitude, different bubble responses are possible. At low pressure amplitudes the bubble response is linear, thereby giving rise to an expression for the linear resonant frequency corresponding to the bubble size. Moderate values of pressure amplitude lead to stable oscillation of the bubble, which in turn gives rise to some interesting bubble phenomena like rectified diffusion and bubble motion in an acoustic field due to Bjerknes forces. Higher pressure amplitude results in transient cavity motion of a bubble; the bubble exhibits a large growth followed by rapid, violent collapse. Several transient cavitation threshold criteria have been proposed (Flynn 1964; Apfel 1981; Arakeri & Chakraborty 1990). When a transient cavity implodes, it may fragment

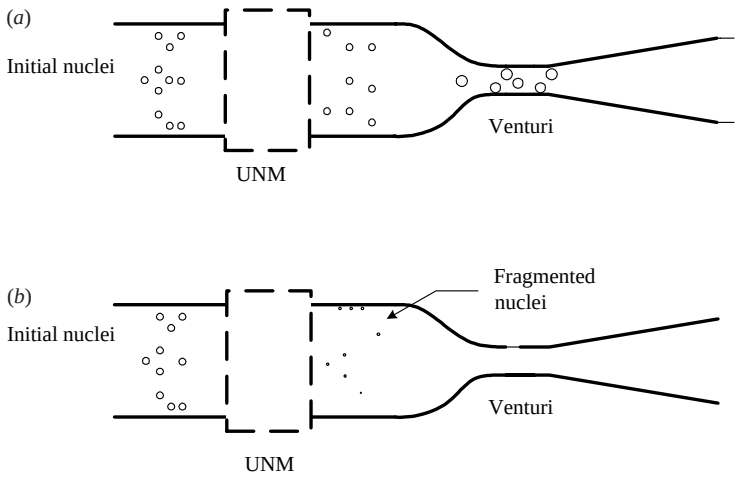

FIGURE 1. A schematic illustrating the use of ultrasonics in hydrodynamic cavitation control. Expected results when the UNM (Ultrasonic Nuclei Manipulator) is (*a*) not used and (*b*) operative. The initial nuclei source can be natural or artificial, like seeding of bubbles by electrolysis.

into several smaller gas bubbles due to the formation of surface instabilities (Flynn & Church 1988; Brennen 2002). This can lead to a proliferation of nuclei in a stagnant liquid, due to acoustic cavitation. Hydrodynamic cavitation, on the other hand, generally requires a continuous supply of nuclei for its sustenance. In the work to be described, we shall exploit this feature to control one form of hydrodynamic cavitation, namely, travelling bubble cavitation (TBC). It is now well established that TBC, among the various types of hydrodynamic cavitation, is the most dangerous type from the view point of noise and damage (see e.g. Brennen 1995).

Motivated by the findings of Flynn & Church (1984), Arakeri & Chakraborty (1990) carried out numerical simulations of the bubble behaviour to predict the potential use of ultrasonics in hydrodynamic cavitation control. The experimental demonstration of the use of ultrasonics in TBC control was done by Chatterjee & Arakeri (1997). The desired control was achieved by introducing a piezoelectric device, termed the *Ultrasonic Nuclei Manipulator* (UNM), upstream of a venturi (as depicted schematically in figure 1). We could demonstrate hydrodynamic cavitation control as follows: first TBC was generated at the throat by having sufficient flow rate through the venturi with electrolysis bubbles being seeded as nuclei, and then the UNM was turned on and the resulting influence was noted. The dramatic effect of the elimination of the existing TBC was clearly established both photographically and by monitoring the noise sensing transducer output. Now the crucial question was, with the UNM on, when will TBC reappear if at all as the flow rate through the venturi is increased beyond the value for cavitation onset. We could not address this question and also some related issues as to whether TBC control is possible under a wide range of operating conditions, for example with developed cavitation; this was due to a major limitation of the apparatus as indicated below. In our previous study, a venturi of high contraction ratio (≈ 100) was used and as a result, the flow in the diffuser region downstream of the throat was laminar. As we tried to obtain lower pressures at the throat, by increasing the flow rate, laminar separation would trigger an attached sheet cavity and this resulted in choking. Basically, the consequence was that the minimum

throat pressure achievable was restricted to a value of about −5 kPa. To overcome this limitation, as part of present study we completely modified the experimental apparatus. First, a low contraction ratio (CR) venturi was used to ensure turbulent flow and thus avoid sheet cavitation. Secondly, we used a gravity-driven set-up as compared to the pressure-driven set-up used previously to generate higher flow rates without experiencing adverse effects, like degassing on the diffuser side. Preliminary studies with the new set-up are described in Chatterjee & Arakeri (2001). Even though the new set-up largely met the intended objectives and allowed us to address some of the questions raised above, the results pointed to a need for careful consideration of some new issues.

One issue related to the use of the UNM with near gas-saturated samples. It was noted that under these conditions, the UNM promoted hydrodynamic cavitation rather than suppressing it. We sought the reasons for this, as well as a remedy, as part of the present study. It turns out that the primary reason is due to the possibility of bubble growth through a mechanism known as *rectified diffusion* (Crum 1984) and the solution to minimize this effect is to use pulsed excitation of the UNM rather than continuous. However, there was a disadvantage with the pulsed mode of operation. In a cylindrical piezoelectric crystal used as the UNM, the acoustic pressure field is non-uniform and near the walls the pressure amplitudes are generally lower than those required for driving the nuclei to prompt transient growth followed by violent collapse. Therefore, nuclei present near the wall are not manipulated unless they are brought to the core by some mechanism. As will be shown later, first theoretically and then experimentally, nuclei migration due to Bjerknes forces (Parlitz *et al.* 1999) with continuous excitation is possible; whereas it is not with pulsed UNM operation. Thus, when the UNM is effective, it appears to be more efficient in continuous mode than pulsed. This then led us to implement two crystals as the UNM, one of them operated in continuous mode and the second in pulsed mode. Definite improvements were observed with two crystals operating in tandem in this manner. This is one of the innovative features of the present work. It should be added that, to systematically study the nuclei migration or movement in a non-uniform acoustic field, we had to use a large crystal and also devise a method to seed nuclei, locally, at different radial locations.

As is apparent, the present work involves the study of nuclei manipulation and in view of this, it would seem appropriate to use a direct method for their observation like holography, laser light scattering or a phase Doppler particle analyser (PDPA). Even though we could have thought of using one of these for characterizing nuclei population ahead of the UNM, similar measurements downstream with some reliability would have been extremely difficult. This is because the fragmented nuclei size estimated on the basis of sustained venturi throat tensions (see § 4.6) is found to be near 1 μm or even smaller. As indicated by Billet (1986), measurement of nuclei of this size range is beyond the general capability of the instrumentation mentioned above. In particular, even if measurements are possible, considerable difficulties are experienced in distinguishing between a bubble and a particle. Thus, the measured nuclei population could even be misleading in terms of their ability to cavitate. It is for this reason that the concept of the use of a cavitation susceptibility meter (CSM) to infer cavitable nuclei has been evolved. Hence, we have preferred a venturi-based set-up along the lines of a CSM for our present study.

Therefore, even though the technique of the use of ultrasonics in hydrodynamic cavitation control was demonstrated by us in a previous study, as indicated above, many basic issues needed to be resolved before considering its application in a

practical device or situation. This forms the focus of the present study. To follow, we first present some numerical evaluation of the effect of the UNM on bubble behaviour with particular emphasis on bubble growth by rectified diffusion and bubble motion under the influence of Bjerknes forces. That is followed by a description of the experimental set-up and instrumentation required to achieve our objectives. Presentation of the results and discussion is then taken up and finally a summary is provided.

2. Numerical study of the effect of the UNM on bubble behaviour

When a liquid sample is subjected to high-intensity ultrasound an acoustic cavitation field is generally established. As pointed out by Leighton (1995), the chemical, physical and biological effects of cavitation depend on two-way interaction between the local sound field and the bubble population as a whole. Therefore, in our application of ultrasound using UNM, it needs to be ascertained whether a single bubble formulation is adequate to predict the transient cavitation and rectified diffusion thresholds and also to quantify the movement of nuclei. A basic difference between the way we have used high-intensity ultrasound from normal application is that the liquid sample flows continuously through the UNM. Thus the evolution of the bubble population is likely to be determined by the nucleus size and number density approaching the UNM; whereas, in a stagnant system, in principle, a single nucleus could trigger a cavitation field through a regenerative mechanism as explained in Leighton (1995). Using the present venturi set-up as a CSM, we have estimated the initial electrolysis bubbles to have size of about 10 μm and their number density to be about $10\,\mathrm{cm}^{-3}$ (see § 4.6). Even if we assume a factor of ten between the total and the unstable nuclei population, the number density ahead of the UNM is $100\,\mathrm{cm}^{-3}$. On the average, one nucleus per $10^{-2}\,\mathrm{cm}^3$ would be expected and the distance between two adjacent bubbles is found to be about 0.26 cm. This distance is quite substantial compared to the maximum radius of about 50 μm of a grown nucleus. Therefore, the bubbles are expected to behave as an isolated entity, thus justifying the use of a single bubble formulation. However, it should be mentioned that with near gas-saturated samples, a bubble population appears to develop within the UNM which is normally observed with stagnant samples. For this reason, under these conditions we had to use pulsed excitation, a technique commonly used to mitigate adverse effects of multibubble interference (Leighton 1995).

Another assumption under which the present computations have been done is to assume a steady forcing in the bubble dynamics equation (see below). In the experimental configuration used here, a nucleus spends about 450 ms within the UNM and under CW excitation it will experience about 8000 cycles during its passage. In the pulsed excitation mode, the number of bursts (see figure 5) used is generally more than 10. It has been pointed out by Flynn & Church (1984) that a cavitation zone from high-intensity ultrasound attains a steady state within about 10 cycles. On this basis, like Flynn & Church (1984), our threshold predictions are based on assuming steady forcing. However, in quantitative predictions like bubble growth and movement, the actual time periods experienced have been incorporated. Thus, for example, the amount of gas entering a bubble from rectified diffusion can be evaluated per cycle by assuming a steady forcing and this rate multiplied by the number of cycles the nucleus experiences then gives the total transport.

Under these assumptions, the radial motion of a single spherical bubble subjected to an imposed sinusoidal pressure field can be computed using bubble dynamics

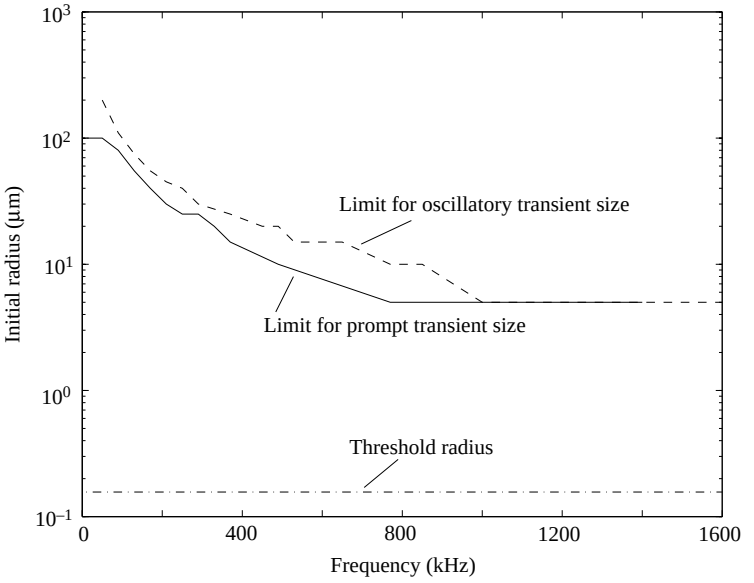

FIGURE 2. Frequency dependence of the bounds for prompt and oscillatory transient cavities. $P_0 = 0.9$ bar and $P_A = 5$ bar. Threshold radius shown is the Blake threshold.

equations valid to various levels of approximation. We have used an equation known as the Rayleigh–Plesset–Keller–Kolodner (RPKL) equation and it is given by (Prosperetti & Hao 1999):

$$\left(1-\frac{\dot{R}}{c}\right)R\ddot{R}+\frac{3}{2}\left(1-\frac{\dot{R}}{3c}\right)\dot{R}^2=\left(1+\frac{\dot{R}}{c}\right)\frac{1}{\rho}\left[P_B-P_s(t)\right]+\frac{R}{\rho c}\frac{\mathrm{d}(P_B-P_s(t))}{\mathrm{d}t}, \quad (2.1)$$

$$P_B = P_g - \frac{2S}{R} - \frac{4\mu}{R}\dot{R}, \quad (2.2)$$

$$P_s(t) = P_0 - P_A \sin(\omega t). \quad (2.3)$$

In the above equations, R, $\dot{R}$ and $\ddot{R}$ refer to the instantaneous bubble radius, wall velocity and acceleration respectively; ρ, S, μ and c denote the liquid density, surface tension, viscosity and sonic velocity respectively; P_g and P_B indicate the pressure of the gas inside the bubble and the pressure in the liquid immediate outside of the bubble wall; $P_s(t)$ refers to the time-varying external acoustic pressure field of frequency f ($\omega = 2\pi f$) and amplitude P_A. The RPKL bubble dynamics equation is of second order; it can be reduced to two first-order equations and solved numerically with $R(t=0) = R_0$ and $\dot{R}(t=0) = 0$ as initial conditions.

2.1. *Determination of suitable operating parameters of the UNM*

One of the objectives of the present numerical investigation was to determine the values for the operating parameters of the UNM (driving frequency and pressure amplitude), for which control of travelling bubble cavitation is expected. Since the basic concept behind the use of ultrasonics in cavitation control is to make the initial nuclei fragment to smaller sizes, we require the UNM to make the nuclei undergo transient cavity motion. The bounds for various thresholds including transient cavity motion are presented in figure 2. It is clearly seen that, as the driving frequency is increased, the range of nuclei lying between the Blake threshold radius and limits for

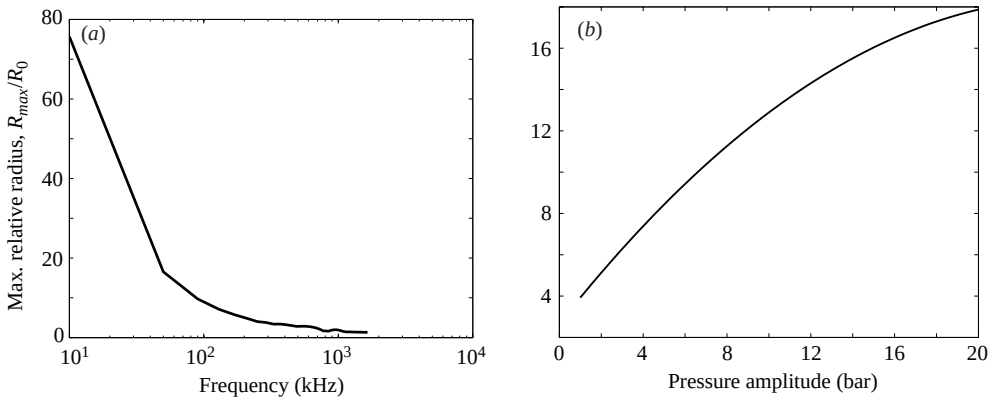

FIGURE 3. Variation of the maximum relative radius with (*a*) driving frequency when $P_A = 5$ bar and (*b*) pressure amplitude with $f = 0.1$ MHz. $R_0 = 10\,\mu$m and $P_0 = 0.9$ bar.

prompt transient motion (or, *capture range* in the words of Arakeri & Chakraborty 1990) reduces. So too high an operating frequency is not desirable.

Next, we present the effect of varying the driving frequency on the maximum relative radius (R_{max}/R_0) for given values of P_A and R_0 (figure 3*a*). It is seen that too low a value of the driving frequency gives rise to higher values of maximum relative radius. Arakeri & Chakraborty (1990) have stated that the typical nucleus size present in a quiescent liquid is between 10 and 20 μm. Hence, an optimum driving frequency for this size range should be around 100 kHz. The effect of increasing the drive pressure amplitude results in an increase in the maximum bubble size attained (figure 3*b*). Therefore, a large value of the acoustic pressure amplitude is undesirable because, for these cases, upon collapse the fragmented nuclei will be larger (Brennen 2002). It may be pointed out in this context that along with these theoretical guidelines, practical issues and constraints will determine the actual driving parameters. For example, a uniform acoustic field, though desirable, may not be feasible. Therefore, the interaction of a bubble with a spatially varying acoustic field is now discussed.

2.2. *Effect of non-uniform acoustic pressure field*

In the present study, as was done earlier (Chatterjee & Arakeri 1997; Chatterjee & Arakeri 2001), a cylindrical piezoelectric crystal driven at its radial resonant frequency has been used as the UNM. As was found earlier, for this crystal configuration there will be a radial variation of the acoustic pressure amplitude inside the crystal. The acoustic pressure amplitude will be a maximum along the axis and a minimum near the wall according to the relation $P_A = P_{A0} J_0(kr)$ where P_{A0} is the acoustic pressure amplitude along the axis ($r = 0$), k is the wavenumber and J_0 is Bessel function. Because of this pressure variation, there could be some regions inside the crystal where the pressure may be lower than the transient threshold limit, but high enough to allow bubbles to grow by rectified diffusion. Thus, we can schematically demarcate the cross-section of the cylindrical piezoelectric crystal into the following three regions (as shown in figure 4*a*):

I. The central core region where the bubbles undergo transient cavitation.

II. The intermediate zone where the bubbles exhibit stable oscillation, and due to the effect of rectified diffusion the bubbles in these locations may grow.

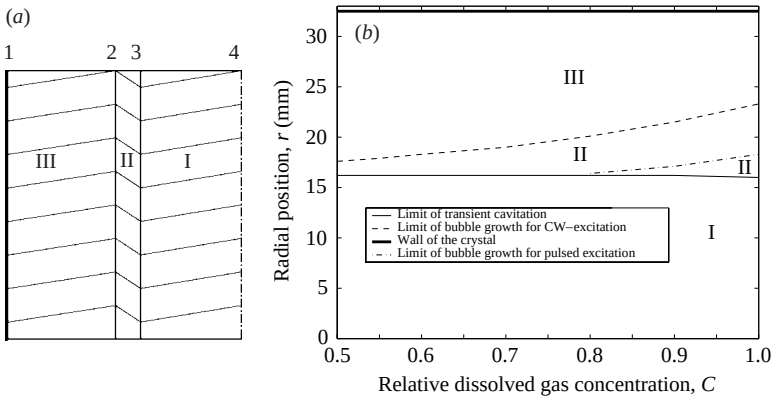

FIGURE 4. Zones of expected different bubble behaviour inside a 3 in. crystal. (*a*) Schematic 1: Wall of the crystal; 4: centreline; 3–4: zone of transient cavitation (zone I); 2–3: zone of bubble growth through rectified diffusion (zone II); 1–2: zone in which bubble shrinks. (*b*) A quantitative picture when $P_{A0} = 1.5$ bar, $P_0 = 0.88$ bar and $R_0 = 10\,\mu$m.

III. The near-wall region where the bubbles oscillate stably and their sizes gradually reduce.

The threshold condition for bubble growth due to rectified diffusion is given by the following equation (Fyrillas & Szeri 1994):

$$\frac{C_\infty}{C_0} - \frac{\langle P(t)\rangle_{t,4}}{P_\infty} = 0. \tag{2.4}$$

Here, C_∞ and C_0 refer respectively to the concentration of dissolved gas in the liquid far away from a bubble and the saturation concentration of the dissolved gas in the liquid at the given temperature; $\langle P(t)\rangle_{t,4}$ denotes the weighted average of $P(t)$ and is given by $\int_0^T P(t)R^4\,\mathrm{d}t / \int_0^T R^4\,\mathrm{d}t$, where T is taken to be equal to 10 periods of the imposed acoustic pressure field. It can be said that a bubble will grow if the expression on the left-hand side of equation (2.4) is positive and shrink otherwise. Using the above threshold criterion for rectified diffusion, for a 10 μm bubble and corresponding to an experimentally observed value of acoustic pressure amplitude (P_{A0}) of 1.5 bar along the axis of a 3 in. crystal, we can demarcate three regions inside the crystal as shown in figure 4(*b*). The method followed to obtain the boundaries between these regions is as follows. Apfel (1981) has defined the transient cavitation threshold as where the maximum bubble radius (R_{max}) attained is $\approx 2.3R_0$. The RPKL equation was solved to obtain values of R_{max}/R_0 attained in a time duration of 10 oscillations. As the initial position of the bubble moves away from the axis, the pressure amplitude it experiences reduces and hence the maximum radius attained decreases. The radial position where $R_{max}/R_0 = 2.3$ gives the boundary of zone I. Beyond zone I, the bubble exhibits stable motion and hence the change of bubble size due to gas diffusion becomes important. The left-hand side of equation (2.4) was evaluated for different dissolved gas concentrations (this quantity is reported here in terms of relative dissolved gas concentration, C, which is defined as the ratio of dissolved gas concentration actually present to the saturated value corresponding to the given temperature of water) and at different radial positions. Depending on the sign of this expression, we could ascertain whether the bubble would grow or shrink in size. This enables the boundary between zones II and III to be identified. The

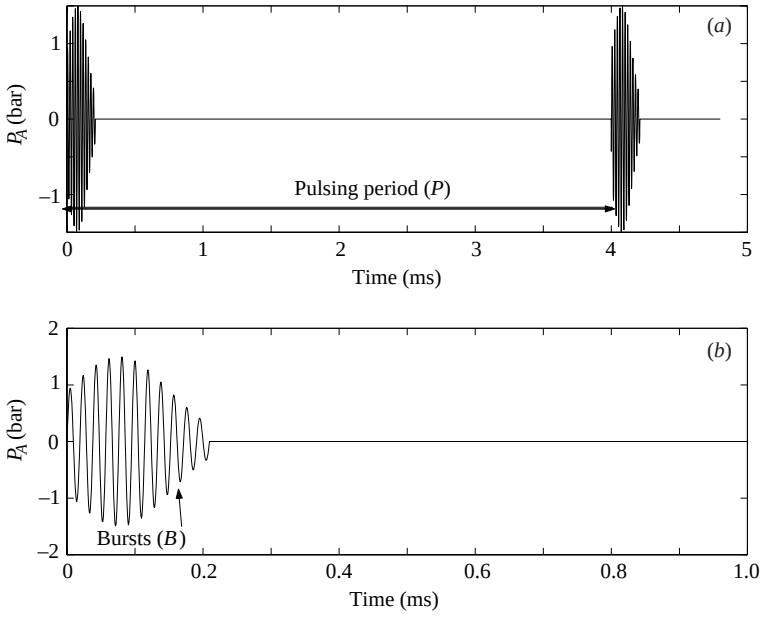

FIGURE 5. Typical pulsed excitation profile of the UNM; (b) a zoomed view of the (a), shows the number of bursts (B).

results presented in figure 4 pertain to two types of excitation of the UNM, namely CW and pulsed modes. In the CW mode, a driving frequency of 18 kHz has been used; whereas, for pulsed excitation, the same frequency was used but with number of bursts, B, as 11 and the pulsing period, P, of 4 ms; see figure 5 for definitions of P and B. It is clear from figure 4 that with an increase in the dissolved gas content of water samples, the zone in which bubbles grow due to rectified diffusion increases. However, as expected this increase is prominent only in the case of CW excitation.

It has already been mentioned that Bjerknes forces may lead to bubble motions in a non-uniform acoustic pressure field. In our case, we have neglected the effects of secondary Bjerknes force since, as pointed out earlier, the nuclei number densities inside the UNM is expected to be low. However, a long duration (450 ms) of stay inside the crystal under CW excitation causes the bubbles to move in response to the radial pressure variation. A quantitative prediction of the bubble migration due to this effect was made following the formulation due to Parlitz *et al.* (1999). The basic equation is:

$$\boldsymbol{F}_M = \boldsymbol{F}_{B1} + \boldsymbol{F}_D, \tag{2.5}$$

where $\boldsymbol{F}_M$, $\boldsymbol{F}_{B1}$ and $\boldsymbol{F}_D$ are added mass force, primary Bjerknes force and drag force respectively. These force terms are

$$\boldsymbol{F}_M = \tfrac{1}{2}\rho\langle V(t)\rangle_T \dot{\boldsymbol{v}}, \tag{2.6}$$

$$\boldsymbol{F}_{B1} = -\langle \nabla P_A(t) V(t)\rangle_T, \tag{2.7}$$

$$\boldsymbol{F}_D = (\beta_1\langle R(t)\rangle_T + \beta_2\langle R(t)\rangle^2{}_T \|\boldsymbol{v}\|)\boldsymbol{v}. \tag{2.8}$$

Here, $V(t)$ refers to the instantaneous bubble volume while $\boldsymbol{v}$ denotes the bubble translational velocity and β_1, β_2 are constants with values $0.015\,\mathrm{N\,s\,m^{-2}}$ and

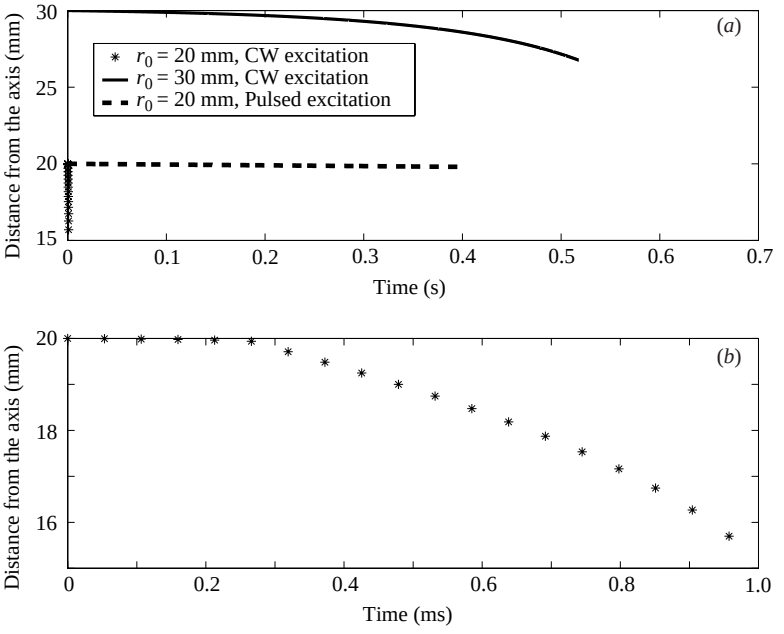

FIGURE 6. Effect of Bjerknes force due to an imposed acoustic field (both CW and pulsed) on the bubble motion inside a 3 in. crystal. r_0 is the initial bubble position. (*b*) A zoomed view of the bubble movement due to CW-excitation when the bubble is initially located at $r = 20$ mm.

4000 N s^2 m^{-3} respectively (Crum 1975). Bubble motion inside the crystal has been computed for both CW and pulsed modes of excitation; the procedure followed is same as that described earlier with reference to the results in figure 4. In figure 6 we present one set of computations based on equation (2.5) and it is clear that under the action of CW excitation, a bubble starting from near the wall may be brought near the core; whereas, with pulsing such a possibility does not exist.

From the numerical studies presented we can state the following. The driving frequency of the UNM should preferably be less than 200 kHz to make the nuclei capture range reasonably high. The maximum acoustic pressure amplitude should not be too high since this will result in larger acoustic cavitation bubbles which could imply bigger fragmented nuclei. There are fundamental differences in the bubble interaction with the acoustic pressure field in the cases of continuous (CW) and pulsed excitation modes. In the CW mode, there is a possibility of nuclei movement from low acoustic pressure amplitude zones (near the crystal wall) to higher acoustic pressure amplitude zones (close to the centre) and this is an advantage in manipulating nuclei sizes from different initial spatial origin. The movement has been traced to the role of Bjerknes force and this effect is nearly non-existent with the pulsed mode of operation. Therefore, in the latter case, the nucleus originating near the crystal wall are unlikely to be manipulated and will contribute to hydrodynamic cavitation. Thus, CW excitation offers a definite advantage over pulsing from this point of view; however, in this mode there is a possibility of nucleus growth due to rectified diffusion with water samples of higher gas concentration, in which case the pulsed mode offers an advantage. Most of the above mentioned features are borne out by experimental findings as will be described later.

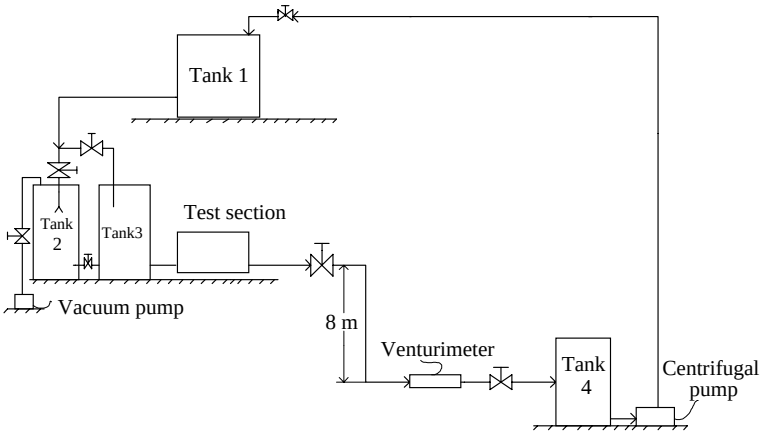

FIGURE 7. Schematic of the overall experimental set-up.

3. Experimental set-up

Figure 7 presents a schematic of the overall gravity-driven set-up. Two large tanks were used as inlet tanks and these were kept at a height of 8 m above the level of the exhaust tank. Tank 2 was of stainless steel and was connected to a vacuum pump. For experiments which required partially degassed water samples, water was sprayed inside this tank under vacuum. Tank 3 served as the final upstream storage point before the water sample flowed through the test section into the exhaust tank (Tank 4). This water was taken back to the overhead tank (Tank 1) using a small centrifugal pump. Near the exhaust tank a venturimeter was placed to measure the flow rate.

3.1. *Test section*

The most important part of the set-up is the test section (figure 8). It consisted of three principal parts, namely the electrodes, the UNM and the venturi. A brief description of each is given below and further details are available in Chatterjee (2002).

Electrodes: A copious supply of nuclei was highly desirable for demonstrating cavitation control by our method. A fine copper wire, used as the cathode, was placed at the end of the bell-mouth connecting Tank 3 with a Perspex tube. The anode was a copper plate (150 mm $\times$ 12 mm $\times$ 4 mm) and was immersed inside Tank 3 (as shown in figure 8). This system enabled the generation of microscopic bubbles (the nominal size of these bubbles, estimated from the critical tension at the throat of the venturi, was found to be around 10 μm) without any appreciable disturbance of the inlet flow. The typical voltage applied across the electrodes was 10 V.

UNM: For the test section used here with a single crystal as the UNM, the ultrasonic pressure field was created by a cylindrical piezoelectric (PZT4) transducer (Morgan Matroc Limited make). This transducer had an outer diameter of 1 in. (25.4 mm), inner diameter of 3/4 in. (19.1 mm) and it was 2 in. (50.8 mm) long. The piezo-crystal was bonded to the Perspex tube on either side by epoxy resin (Araldite). To facilitate proper bonding at the joint, tie rods were connected between the flanges mounted on the Perspex tubes located on either side of the crystal. The cylindrical crystal had silver coatings on its inner and outer surfaces and these served as the electrodes. An obvious choice for the driving frequency of the UNM could be the crystal resonant frequency. This, for the cylindrical PZT crystal used as the UNM, can be either the fundamental radial or the thickness mode resonant frequencies.

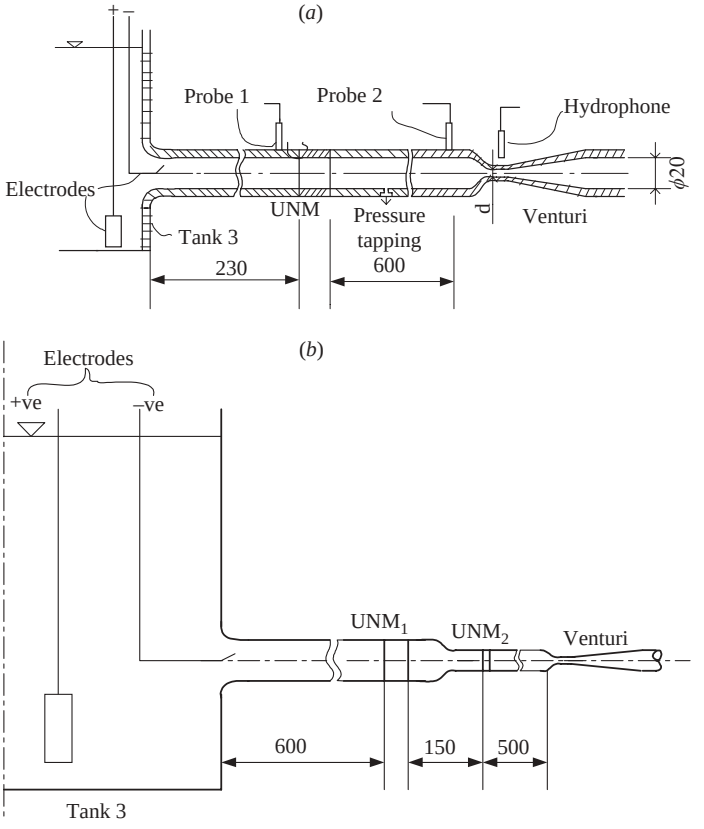

FIGURE 8. Typical test section: (*a*) the set-up with one crystal and (*b*) indicates a test section with two crystals. All dimensions in mm. Not to scale.

It should be pointed out here that the thickness mode frequency is always much higher (typically about 700 kHz for this crystal) than the radial mode and it has been shown in figure 2 that a higher operating frequency would result in a shrinkage of the capture range of nuclei. Hence, for our experiments, the UNM was driven at its radial resonant frequency (breathing mode) of 52 kHz as determined from the manufacturer's catalogue. Another possible driving frequency could be the system resonant frequency accounting for the crystal and the Perspex tubes. But as discussed earlier in Chatterjee & Arakeri (1997), from the point of view of cavitation control, using the crystal resonant frequency is more appropriate than the system resonant frequency.

Two crystals: Based on our experience with a single 1 in. crystal, it was seen that it is essential to seed nuclei at specified radial locations for a clearer picture of the interaction between the bubbles and the acoustic field. This was achieved by using a bigger crystal in conjunction with the smaller one. The second crystal (Morgan Matroc Limited make) had an outer diameter of 3 in. (76.2 mm), an inner diameter of 2.5 in. (65 mm) and was 4 in. (101.6 mm) in length (see figure 8). The second, larger, crystal, placed upstream of the smaller one, was also driven at its fundamental breathing mode frequency (18 kHz). It should be noted here that the bigger crystal could be operated properly by introducing a matching inductor in series with the crystal and

its instrumentation. The value of the inductor used (1.5 mH) was estimated following the procedure outlined in Heuter & Bolt (1955).

Venturi: Venturis were used to generate travelling bubble cavitation in the present experiments. For a venturi, the critical design parameters are the contraction ratio, contraction and expansion angles. High contraction ratios will ensure larger velocities at the throat. However, a very high contraction ratio may lead to relaminarization of the flow which in turn may cause flow separation in the diffuser. We had experienced this difficulty in our previous study (Chatterjee & Arakeri 1997). All the venturis used in the present studies had a contraction angle (half-angle) of 12°. A high value of expansion angle could result in separation and a small value could mean a larger pressure drop. Thus, as a compromise, the expansion angle (half-angle) was chosen as 2.5° for all the venturis tested.

Venturis with two different contraction ratios were used in the present experiments. We started with a venturi having a contraction ratio of 3 and throat diameter of 10.9 mm (referred to as venturi-1). This venturi produced some of the desired experimental conditions; however, natural nucleus cavitation at the venturi throat could not be achieved because of the restricted range of tension possible at the throat location. Hence, in some of the later experiments we used a venturi of contraction ratio of 6 with a throat diameter of 7.7 mm (referred to as venturi-2). Unless there is a need, the results in later sections will be presented without specifically mentioning the venturi used.

Cavitation noise from near the venturi throat was picked up by a wall-mounted subminiature pressure transducer (PCB 112A21); this is designated as Probe 2 in figure 8(*a*). A miniature hydrophone (B & K 8103) was used to detect the air-borne noise; this could also be used to establish the crystal resonant frequency prior to each set of experiments. It may be noted here that to suppress the contamination of the cavitation-noise sensing transducers from the acoustic excitation of the crystal, a carefully designed notch filter was used. The reference static pressure used to calculate the cavitation number (σ), as defined later, was measured by a differential pressure transducer (PD1-HBM). Another, similar differential pressure transducer was connected across the venturimeter, located near the exhaust tank, to measure the discharge.

The driving-side instrumentation consisted of instruments required to drive the UNM and that required to produce electrolysis bubbles. A power amplifier (B & K type 2713), a function generator (Wavetek model-29) and a sine generator (B & K type 1051) were used to drive the UNM while a DC voltage source (Aplab 7711) was used to produce electrolysis bubbles. The data acquisition and processing was done using a computer based data acquisition system (DAS). Further details of the instrumentation system used here can be found in Chatterjee (2002).

4. Experimental results and discussion

We shall first define the cavitation number, σ, used throughout the presentation of the results:

$$\sigma = \frac{P_0 - P_v}{\frac{1}{2}\rho V_t^{\,2}}. \tag{4.1}$$

Here, P_0 and P_v refer to the upstream static and vapour pressures respectively and V_t denotes the velocity at the throat of the venturi. Here, P_0 was measured using a pressure transducer, V_t was obtained from the measured flow rate and P_v was

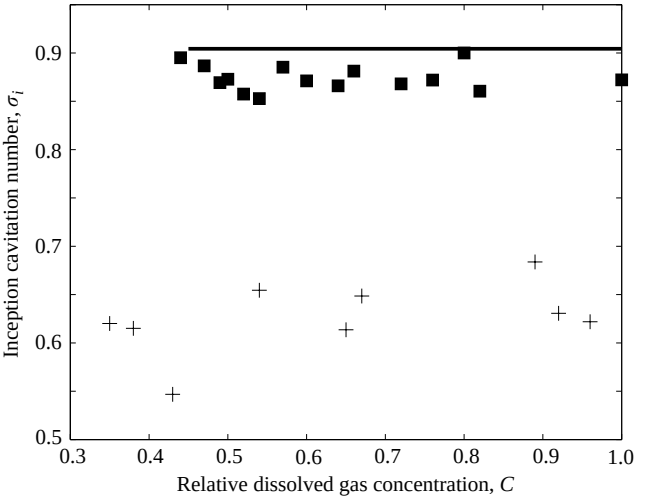

FIGURE 9. Variation of inception cavitation number (σ_i) with the dissolved gas concentration: —, theoretical $(-C_p)_{min}$; ■, inception due to electrolysis bubbles; +, inception due to natural nuclei.

obtained from standard tables. In the presentation of the results, we shall normalize respective σ-values with the inception value corresponding to those obtained with the seeding of electrolysis bubbles, σ_{ei}. In figure 9, cavitation inception data as obtained using venturi-1 are presented. The results for venturi-2 were very similar. It is clear from the results presented that, with a copious supply of nuclei, the inception index denoted by σ_{ei} is very close to the negative value of the theoretical minimum pressure coefficient, $-C_{p_{min}}$, whereas with natural conditions the σ_i values are much lower, signifying the ability of the water sample to sustain tension. It should be mentioned that in the present set-up, where the liquid sample was allowed to sit under quiescent conditions for several hours before the commencement of an experimental run, both the size and the number density of natural nuclei are expected to be small. In fact, the nuclei under these conditions may even be in the form of particulates rather than gas bubbles. Therefore, the results shown in figure 9 are along the expected lines and they also establish that the choice of the design parameters for the present venturis, the methodology used for defining inception and the basic instrumentation used were satisfactory.

4.1. *Effect of an increase in the driving voltage of the UNM at* $\sigma \approx \sigma_{ei}$

One of the objectives of the present study was to arrive at the working parameters (driving frequency and acoustic pressure amplitude) of the UNM. The driving frequency, as indicated earlier, was selected to be the breathing mode of the piezoelectric crystal used as the UNM. A suitable driving voltage (V_{inp}) then needs to be ascertained in order to achieve cavitation control. Towards this end, using venturi-1, we have studied the effect of changing the driving voltage at $\sigma \approx \sigma_{ei}$ for different values of relative dissolved gas concentration (C). The compiled results are shown in figure 10. This figure shows that for $C > 0.7$, the voltage at which there is an increase in noise levels is lower than that required for control. Hence, for these higher C values control is not expected to be possible with CW excitation. Based on the numerical results presented in § 2, we suspect seeding of nuclei by the UNM with

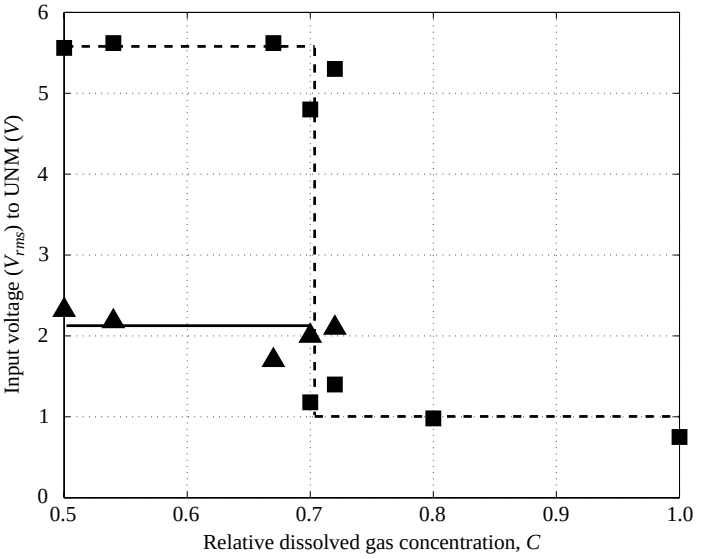

FIGURE 10. Influence of input voltage on the UNM performance: ■, voltage at which there is an increase in the noise level; ▲, minimum voltage at which there is control. When the former is less than the latter, control is not possible.

$C > 0.7$ due to bubble growth by rectified diffusion and a method to overcome this was to use pulsed excitation.

4.2. *Effect of changing the nature of excitation of the UNM at* $\sigma \approx \sigma_{ei}$

Preliminary results (Chatterjee & Arakeri 2001) indicated that, unlike CW excitation, the pulsed mode of excitation controlled travelling bubble cavitation uniformly over the entire range of C. This point was clear from the qualitative results obtained in the form of time traces of the Probe-2 signal as presented in the previously cited study. Here, we have quantified these findings over a much wider range of operating conditions by using a counter system. The instrumentation used is standard in nuclear applications and consisted of an EG & G ORTEC amplifier and discriminator (Model 9302) and a counter (Model 770). By setting an appropriate discriminator level we could count the number of events (from the transducer signal) which crossed a certain threshold; this threshold value was set just above the maximum signal level obtained in the absence of cavitation, thus eliminating non-cavitating flow noise. The outcome of these measurements is presented in terms of a number ratio (N) which is defined as the ratio of the number of occurrences (above the set threshold) in some time interval when the UNM is on to that obtained in the same duration of time when the crystal is off. Thus symbolically, $N = N_{on}/N_{off}$. Thus, a lower value of N signifies greater control, whereas, $N > 1$ implies that the UNM is enhancing cavitation activity at the venturi throat. In figure 11 we present a comparative picture of the extent of control achievable by the two modes of excitation. This plot clearly brings out the important role played by pulsed excitation, using which control is possible over a wide C range. This observation conforms to the numerical predictions presented earlier. Basically, due to the limited time of exposure under pulsed excitation, possible bubble growth due to rectified diffusion is suppressed.

It has been shown in figure 5 that two parameters which characterize the pulsed mode of excitation of the UNM are the period of pulsing (P) and the number of

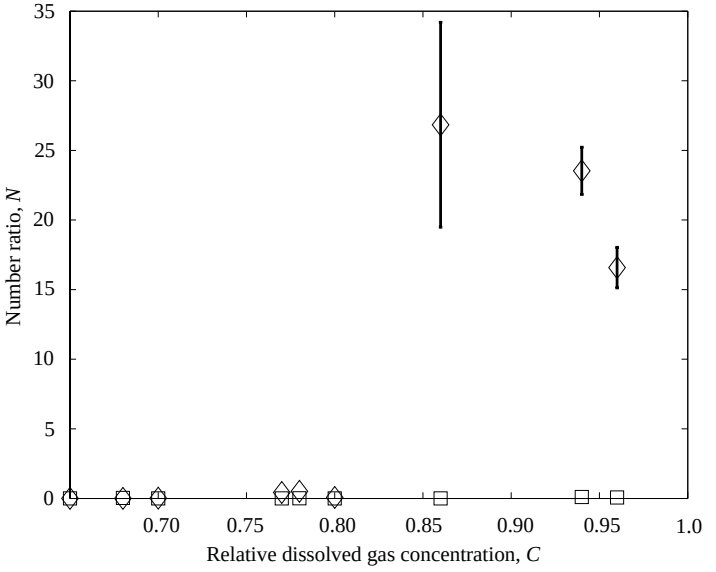

FIGURE 11. Effectiveness of CW and pulsed ($P = 4$ ms and $B = 11$, see figure 5 for definition of P and B) modes of excitation of the UNM in controlling travelling bubble cavitation at the venturi throat. $\sigma \approx \sigma_{ei}$ and electrolysis is on. ◇, Continuous-wave excitation (CW); □, pulsed excitation. Where error bars are not shown explicitly, they lie within the symbol size. $N = 0$ implies complete control; $0 < N < 1$ implies partial control and $N > 1$ indicates lack of control and seeding of nuclei by the UNM.

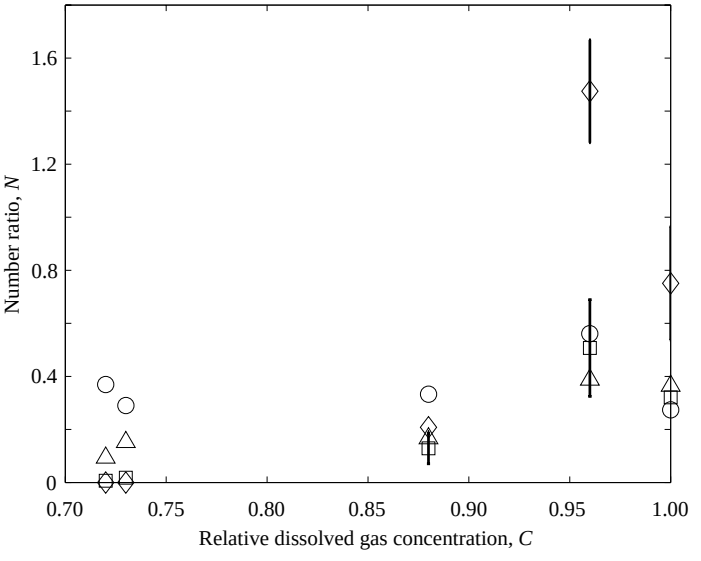

FIGURE 12. Effectiveness of different values of period (P) when the number of bursts (B) is held constant at 11 in case of pulsed excitation of the UNM. $\sigma \approx \sigma_{ei}$ and electrolysis is on. ◇, $P = 1$ ms; □, 4 ms; △ 8 ms; ○, 12 ms. Where error bars are not shown explicitly, they lie within the symbol size. See caption of figure 11 for significance of various values of N.

bursts (B) in each cycle. Better control may be achieved if we could arrive at an optimum combination. The results from the optimization studies by varying P are presented in figure 12. From this plot it is clear that a pulsing period of 4 ms gives

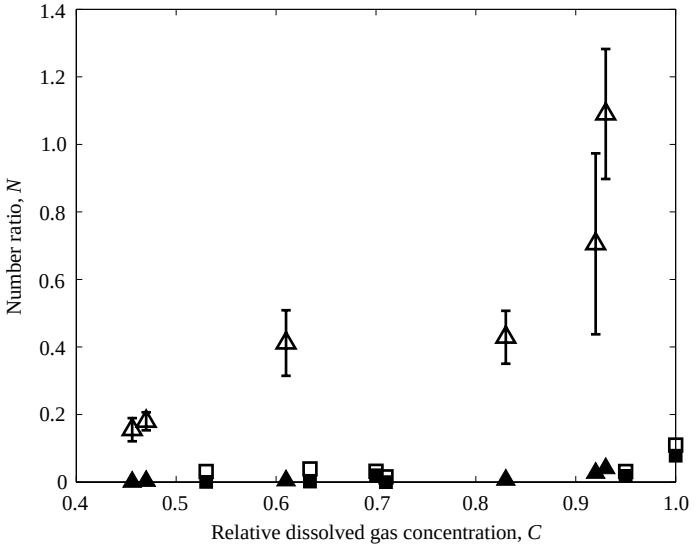

FIGURE 13. Comparison of the effectiveness of CW and pulsed excitations of the big (3 in.) crystal when nuclei are seeded at different radial (r) locations. ■, $r = 0$ mm, CW excitation; ▲, $r = 30$ mm, CW excitation; □, $r = 0$ mm, pulsed excitation; △, $r = 30$ mm, pulsed excitation. Where error bars are not shown explicitly, they lie within the symbol size. See caption of figure 11 for significance of various values of N.

the best result. Similar studies by varying B indicated that the best value for the number of bursts is $B = 11$ (Chatterjee 2002). Therefore, $P = 4$ ms and $B = 11$ seems to be the optimum combination for the crystal and the drive parameters used here. It should be apparent that one may find different values if the UNM configuration is varied. In particular, we expect that the optimum value of P, P_{opt}, will be related to the residence time, T_{res}, of the nuclei in the UNM.

4.3. *Experiments with nuclei seeding at different radial positions*

We have shown the importance of the dissolved gas content in the effectiveness of the CW mode of the UNM operation and have suggested pulsing as a remedial measure when the water sample is near saturation. However, we noticed a curious feature that the relative control with medium or lower C values was better with CW excitation than pulsed. It was suspected that this is related to the issue of nuclei movement as discussed at the end of § 2. Therefore, in order better to understand the influence of the UNM under different operating conditions, we investigated in some detail the interaction of a nucleus with the imposed acoustic field by seeding electrolysis bubbles at definite radial locations. Experiments were conducted by driving the 3 in. crystal in CW and pulsed modes and by seeding electrolysis bubbles at initial radial locations of 0, 20 and 30 mm from the axis of the crystal. The results which capture the essential features are presented in figure 13. From these results it should be noted that the effectiveness of CW excitation is similar for electrodes (cathode) located at extreme radial locations of 0 and 30 mm. With pulsing, on the other hand, it is seen that the extent of control achievable is sensitively dependent on the radial location of nuclei seeding; the UNM performance deteriorates very fast as the electrode moves away from the axis. Therefore, these results clearly support our conclusions based on the numerical computations (see figure 6) that nuclei movement due to Bjerknes force

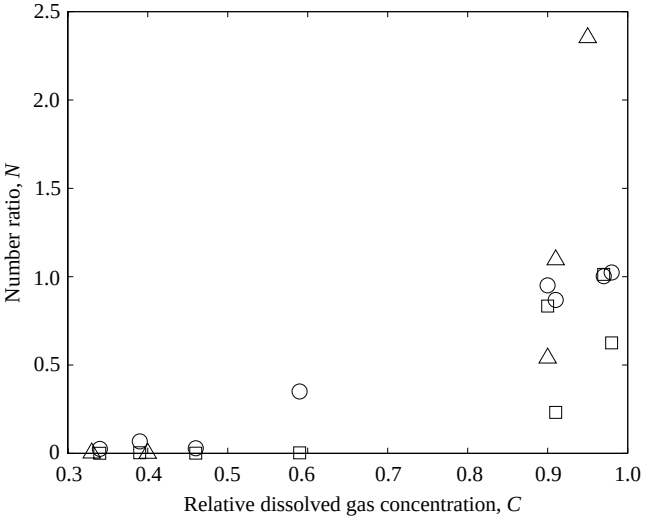

FIGURE 14. Comparison of the effectiveness of using various combinations of excitations of the two crystals (small and big): ○, big (C); □, Big (C) + small (P); △, small (C). big (C) and small (C) denote respectively big and small crystals operated in CW-excitation and small (P) denotes small crystal operated in pulsed mode with $P = 4$ ms and $B = 11$. Electrolysis is on. Error bars have not been indicated to retain clarity but they are of similar magnitude as in figures 11, 12 and 13.

can be a significant factor in the effectiveness of the UNM in controlling cavitation with different modes of crystal operation.

4.4. *Use of multiple crystals as the UNM*

From the results presented so far it can be noted that CW and pulsed modes of operation possess certain advantages and also suffer from some disadvantages. Pulsing seems to be an ideal choice to avoid undesirable effects of rectified diffusion associated with the CW excitation of the UNM in near-saturated water. But, performance under pulsed excitation was adversely affected because the nuclei present away from the axis escape manipulation. This problem was circumvented by a novel approach of using the big and small crystals in tandem. CW excitation of the big crystal, located upstream of the small one (see figure 8), was used not only to destroy the centrally located bubbles but also to bring the nuclei from near the wall to regions close to the axis. These nuclei will then be acted upon by the small crystal, producing a further reduction in the number of cavitable nuclei. A quantitative comparison of the effectiveness of the two-crystal combination and the use of single crystals individually is depicted in figure 14. It can be seen that a combination of the big (3 in.) crystal operating in the CW mode and the smaller one (1 in.) in pulsed mode reduces noise more effectively than use of a single crystal, irrespective of the dissolved gas concentration. Photographs of cavitation at the venturi throat under different experimental conditions where the big and small crystals have been used individually as well as in conjunction are presented in figure 15. The tandem use of the crystals is clearly superior and hence these photographs support our quantitative results.

4.5. *Alternative measures of travelling bubble cavitation control*

The results we have presented in the previous sections pertain to the use of the UNM when the extent of cavitation induced by seeding electrolysis bubbles was limited or

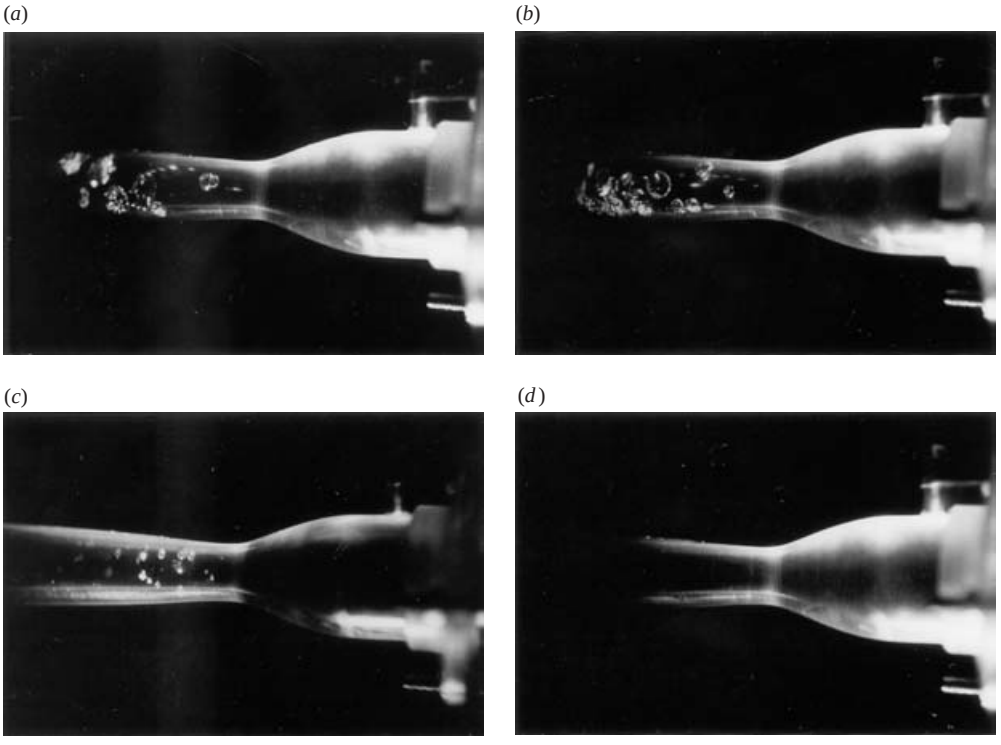

FIGURE 15. Cavitation at the throat of venturi-2. $C = 0.85$, $\sigma \approx 0.9\sigma_{ei}$ and electrolysis is on. The conditions for the photos shown are: (*a*) no crystal; (*b*) only the big crystal (*c*) only the small crystal (*d*) both the crystals are operative. The big crystal is driven in CW excitation while the small one is pulsed. The flow is from right to left.

implying operating at $\sigma \approx \sigma_{ei}$. It was of interest to see if the UNM can be effective in controlling cavitation when it is in more developed state or with $\sigma < \sigma_{ei}$. Some experiments in this direction were done by using the 1 in. crystal as the UNM. The flow rate in the venturi was first adjusted so that the σ value was close to σ_{ei}, then it was increased such that σ was reduced, which resulted in more developed cavitation at the venturi throat. Thus, an attempt was made to reduce σ by increasing the flow rate, and at the same time the effectiveness of the UNM was tested by turning it on and off periodically but driven under CW mode when on. This procedure allowed a comparison of the state of cavitation, as gauged from the noise-sensing transducer signal, when the UNM is turned on or off at given (reduced) σ values. One set of results (additional results are available in Chatterjee 2002) from such a study are presented in figure 16. The top plot (*a*) shows the σ value variation with time or as the flow rate is gradually increased; (*b*) shows the time when the UNM is turned on and finally (*c*) shows the cavitation noise-sensing transducer signal. Some significant observations can be made from the results presented in figure 16. The first is that the effectiveness of the UNM in controlling cavitation is present with developed cavitation but it is reduced as the σ value is decreased. The second, very important, observation is that the lowest cavitation number achievable is appreciably reduced when the UNM is turned on; this is evident from the dips in σ values at later times in figure 16(*a*). This shows that the choking of the system due to venturi cavitation can be postponed with

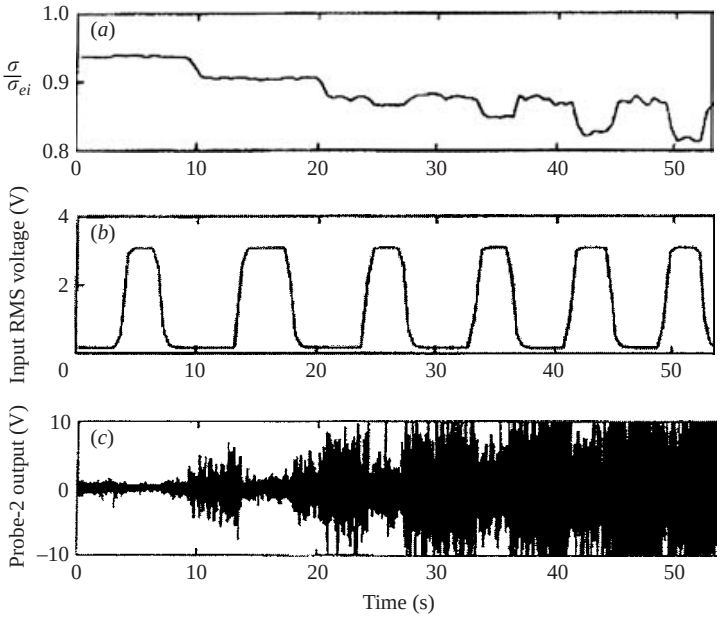

FIGURE 16. Plots to show the effectiveness of the UNM at various cavitation numbers; $C = 0.54$ and electrolysis is on. (*a*) The variation of cavitation number. (*b*) The UNM status: it is on when the input RMS voltage is about 3 V, otherwise it is off. When on, the UNM is in CW excitation. (*c*) The corresponding transducer signal.

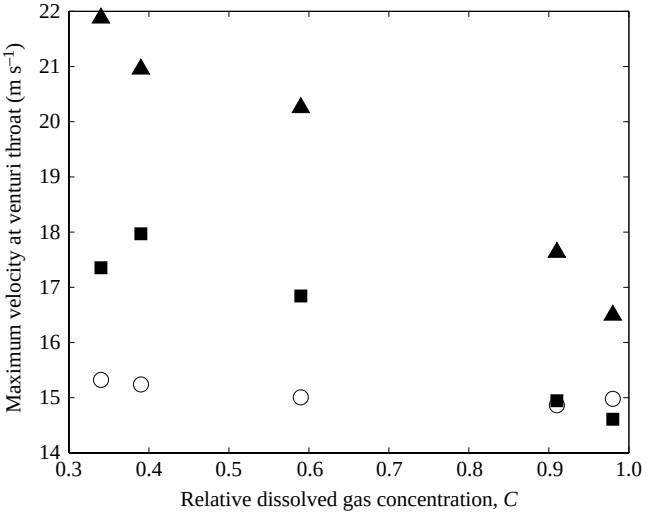

FIGURE 17. Effect of the UNM on the maximum possible velocity at the venturi throat. Electrolysis is on: ○, without the UNM; ▲, big (C) and small (P); ■, big (C).

the use of the UNM or in another words, the maximum attainable throat velocity is increased.

We could quantify this observation as an alternative measure of cavitation control and the results are presented in figure 17. As in the case of noise reduction near inception conditions, here also we find that a combination of CW excitation of the

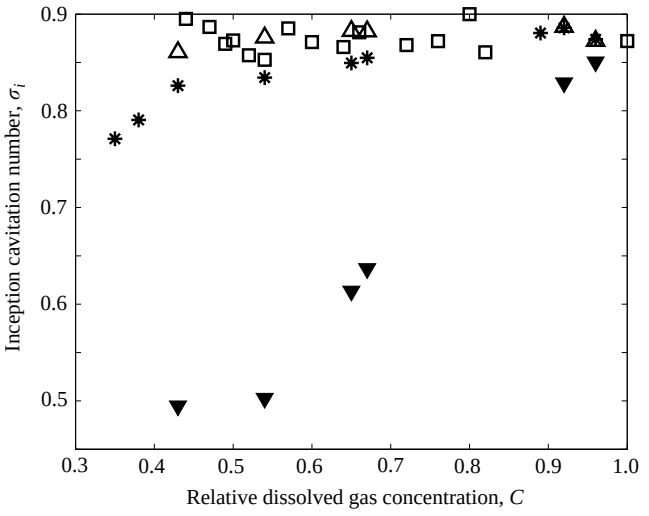

FIGURE 18. Comparison of inception cavitation numbers obtained using various combinations of excitations of the UNM. Here the big crystal is driven in CW mode and the small one is pulsed: □, electrolysis only; ∗, electrolysis and big crystal; △, electrolysis and small crystal; ▼, electrolysis and two crystals.

big crystal in conjunction with pulsing of the small crystal works best. It is noted that the maximum velocity attained is $22\,\mathrm{m\,s^{-1}}$ when $C = 0.35$ and $17.5\,\mathrm{m\,s^{-1}}$ at $C = 0.9$ when this combination is used; the corresponding value in the case of not using the UNM it is about $15\,\mathrm{m\,s^{-1}}$. It should be noted that an increase in the throat velocity, or equivalently the maximum flow rate, is possible by partial control of cavitation, due to a reduction in the number density of cavitation bubbles. Following d'Agostino & Acosta (1991), it is possible to calculate the number density of unstable nuclei at different throat pressures and the results of such an exercise will be presented in the next section. A more stringent alternative measure of the ability of the UNM in manipulating nuclei would be its effect on inception. Therefore, we look for a delay in the inception due to the activation of the UNM, which we could term the *margin* for control; however, in this case it is total and not partial. The effect of the UNM on the value of σ_i is presented in figure 18. Here, the efficiency of the use of the two crystals as the UNM is clearly shown. The reductions are impressive, being almost 50% at low C values. More modest reductions are observed with the use of single crystal as the UNM at all C values and also with C values near saturation with the use of any UNM. Improvements definitely need to be made to make the UNM more effective at higher dissolved gas concentration. One possible method is to increase the residence time of manipulated nuclei between the UNM and the venturi, the site of cavitation.

4.6. *Use of venturi as a cavitation susceptibility meter*

Our venturi set-up could be used as a cavitation susceptibility meter (CSM), for example, along the lines of Oldenziel (1982) and d'Agostino & Acosta (1991) to extract some information on the concentration of the unstable nuclei responsible for the observed cavitation. This was possible by counting the number of cavitation events at a known cavitation number or equivalently the known throat pressure. With

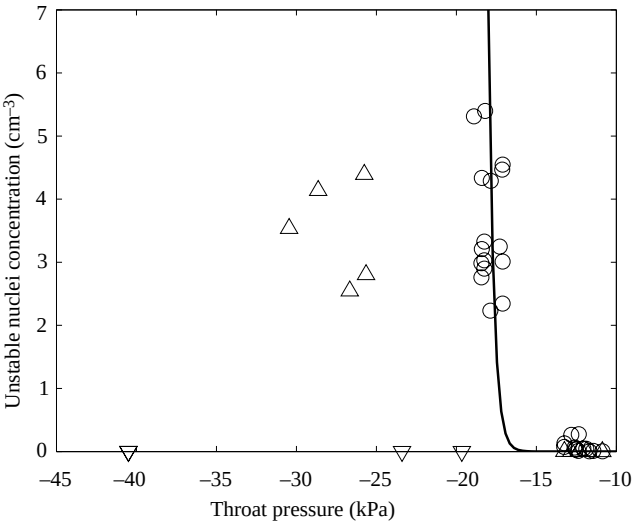

FIGURE 19. Variation of the concentration of unstable nuclei with throat pressure under different operating conditions of the UNM: ○, UNM off; △, pulsed excitation of the small crystal; ▽, combination of two crystals – big crystal in CW excitation and small one pulsed. Solid line shows an exponential curve passing through the data obtained in the absence of the UNM. In all the cases, electrolysis is on. Each data point represents an average of three observations.

knowledge of the flow rate, these numbers could be translated to unstable nuclei concentration values following the procedure outlined in d'Agostino & Acosta (1991). Some results thus obtained are presented in figure 19. Consider first the case of results with electrolysis bubble seeding, but without the operation of the UNM. It is seen that at some throat pressure, there is an exponential growth in the unstable nuclei concentration with further increase in throat tension. This is consistent with previous observations and at a critical tension, coincident with the almost vertical rise of the exponential curve, the venturi chokes, meaning no further increase in throat tension is possible. The maximum nuclei concentration measured seems to be of the order of $6\,\mathrm{cm}^{-3}$. With the use of a single crystal as the UNM, the general behaviour is similar to the case just discussed, but the vertical rise now occurs at a larger throat tension, thus signifying modification of both size and number density of nuclei downstream of the UNM. With two crystals as the UNM, there is a dramatic change in the general behaviour; in this case no cavitation events are detected even with a throat tension of 40 kPa. It should be noted that this value is almost three times larger than the limiting tension possible without the use of the UNM and almost ten times the limiting tension we could achieve in our previous study (Chatterjee & Arakeri 1997). Using the value of the pressure of -40 kPa in an expression derived from static stability analysis (see for e.g. Arakeri & Chakraborty 1990), the value for the radius of the unstable nucleus was found to be about 1 μm. Therefore, even though about 10 μm bubbles were seeded, the UNM is able to reduce their size to at least 1 μm. As pointed out earlier, it should be noted that the measurement of nuclei of this size, and in particular, to distinguish between a bubble and a particulate, is extremely difficult if not impossible by using the standard optical techniques for nuclei sizing (Billet 1986).

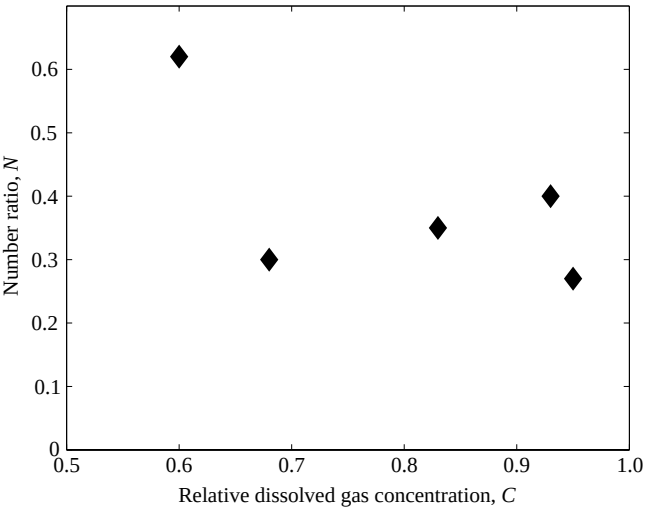

FIGURE 20. The extent of the control of cavitation due to natural nuclei achievable with the use of the small crystal in pulsed mode with $\sigma/\sigma_{ei} \approx 0.59$.

4.7. *Additional remarks*

Before summarizing our results we would like to touch upon two additional aspects (*a*) the use of the UNM in cavitation control with different sizes of nuclei, in particular with natural nuclei and (*b*) the potential applications of the technique. The question of natural nuclei is somewhat awkward since the size and number density of nuclei can vary not only from facility to facility but also in the practical environment. Natural nuclei to the extent currently produced by seeding of electrolysis bubbles are possible in some water tunnel facilities not having resorbers and similarly a copious supply of nuclei can exist in the ocean near the surface. On the other hand, nuclei supply would be limited in the oceans at greater depths and also in water tunnel facilities possessing efficient resorbers. In the present experiments without seeding of electrolysis bubbles, the nuclei content is expected to be quite limited since the water sample was left sitting for few hours before the commencement of the tests and thus the conditions are expected to be the other extreme to those of copious supply generated by seeding of nuclei. Therefore, if the UNM is found to be effective even under natural nuclei conditions then we can be fairly confident of its potential use in different practical environments. The typical results obtained with the use of the UNM under these conditions are presented in figure 20. It is established that the UNM is effective in controlling cavitation even with natural nuclei since the value of N is always less than 1.

Therefore, with this finding and along with our present and previous results with nuclei seeding, we have demonstrated that hydrodynamic cavitation control using ultrasonics is possible with a wide range of initial nuclei sizes. Even though the seeded nuclei in the present work had a limited size range, in the earlier study (Chatterjee & Arakeri 1997) it was much larger. In that study, electrolysis bubbles were generated from a copper wire of about 160 μm in diameter and it essentially spanned the upstream section. Based on measured size range of electrolysis bubbles produced from a 50 μm wire by Kodama *et al.* (1979), the expected size range from a 160 μm wire is from 16 to 160 μm, which was confirmed with limited photographic observations. Hydrodynamic cavitation control was possible with this initial nuclei size range; we

might point out that this is also expected from our numerical study of thresholds presented in figure 2. Basically, at the UNM operating frequency of about 52 kHz, the size range between the Blake threshold and the prompt transient threshold is from less than 1 μm to slightly in excess of 100 μm. Nuclei in this capture range are expected to be manipulated, enabling hydrodynamic cavitation control.

Next we mention certain potential applications for the use of ultrasonics in hydrodynamic cavitation control. One possible application could be in liquid sodium-cooled Fast Breeder Reactors (FBR). Avoidance of cavitation is quite important here since it is proposed to detect voidage from boiling in the core using acoustic means. The UNM could be placed at any convenient location in the coolant pipe and the fact that the coolant in the FBR operates in a closed path could be an added advantage in the light of the fact that the liquid sample will make multiple passes through the UNM. Barger (1964) has found that under such conditions certain types of nuclei can be destroyed by repeated ultrasonic cavitation. Our results with multiple crystals also tend to support this. It was seen here that the maximum flow rate attainable in a system could be increased under the influence of the UNM. This implies that this approach to cavitation control could find applications in increasing the operating range of a venturimeter. Another potential application could be related to the use of hydrodynamic cavitation in the emerging field of sonochemistry (Moholkar & Pandit 2001). The UNM could be utilized for generating and manipulating nuclei for increasing the efficiency of cavitation-induced sonochemical reactions.

All these applications would require additional power input to the UNM and an estimate for this would be in order. For example, in our experiments the measured power inputs to the crystals at their operating conditions are 22 W for the small crystal and 62 W for the large one; in terms of power densities these correspond to $0.6\,\mathrm{W\,cm^{-2}}$ and $0.3\,\mathrm{W\,cm^{-2}}$ respectively. It has also been shown (Chatterjee & Arakeri 1997) that the effect of acoustic pre-cavitation at the UNM location is negligible in terms of harmful effects when compared to travelling bubble cavitation. Thus, on the whole, it can be argued that the gains due to primary hydrodynamic cavitation reduction in a practical device should outweigh the added energy cost and risks involved with the operation of the UNM.

5. Summary

Our earlier studies on hydrodynamic cavitation control revealed the potential use of ultrasonics through experimental demonstration. However, several important issues had remained unresolved. For example, we could not determine the margin – the delay in the onset of cavitation – that could be achieved using ultrasonics. The characteristics and effectiveness of the ultrasonic nuclei manipulator (UNM) in controlling cavitation under developed cavitation conditions and with natural nuclei could not be tested. In this work, we have addressed these issues. We have also quantified the extent of reduction in cavitation-induced noise achievable under different operating conditions by using a counter-based instrumentation system. It has been shown that for a saturated water sample, the pulsed mode of excitation offers better control; however, for low levels of gas concentration, CW excitation should be the preferred mode of the UNM operation. We have designed a suitable experimental set-up to bring out the roles played by rectified diffusion and Bjerknes force in the effective use of the UNM. The numerical results lend good support to our experimental findings on this aspect. We could show a reduction in noise due to cavitation from natural nuclei and thus it has been demonstrated that the use

of ultrasonics in hydrodynamic cavitation control is possible under a wide range of initial nuclei population. Alternative measures of cavitation control, such as the question of delay in inception (the margin) and an increase in the maximum flow rate attainable in the system, have been investigated. Use of multiple crystals as the UNM seems to produce better control under all experimental conditions and for all measures of cavitation control – noise, margin and the maximum flow rate attainable. Additional consumption of power by the UNM appears to be a small price to pay in order to check the harmful effects of uncontrolled hydrodynamic cavitation.

We would like to thank P. Govindaraju for expert fabrication of the experimental components and for assisting in conducting the experiments. We would also like to thank Murali R. Cholemari for helping us in the photography of cavitation events.

REFERENCES

d' Agostino, L. & Acosta, A. J. 1991 A cavitation susceptibility meter with optical cavitation monitoring— part two:experimental apparatus and results. *Trans. ASME: J. Fluids Engng* **113**, 270–277.

Apfel, R. E. 1981 *Acoustic Cavitation*, *Methods Expt. Physics* (ed. P. D. Edmonds), vol. 19, pp. 355–411. Academic.

Arakeri, V. H. & Chakraborty, S. 1990 Studies towards potential use of ultrasonics in hydrodynamic cavitation control. *Current Sci.* **59**, 1326–1333.

Barger, J. E. 1964 Thresholds for acoustic cavitation. *Tech. Rep.* 59. Acoustics Research Laboratory, Harvard University.

Billet, M. 1986 The importance and measurement of cavitation nuclei. In *Advancements in Aerodynamics, Fluid Mechanics and Hydraulics* (ed. R. E. A. Arndt, H. G. Stefan, C. Farell & S. M. Peterson), pp. 967–989. ASCE.

Brennen, C. 1995 *Cavitation and Bubble Dynamics*. Oxford University Press.

Brennen, C. E. 2002 Fission of collapsing cavitation bubbles. *J. Fluid Mech.* **472**, 153–166.

Chatterjee, D. 2002 Some investigations on the use of ultrasonics in hydrodynamic cavitation control. PhD thesis, Indian Institute of Science, Bangalore, India.

Chatterjee, D. & Arakeri, V. H. 1997 Towards the concept of hydrodynamic cavitation control. *J. Fluid Mech.* **332**, 377–394.

Chatterjee, D. & Arakeri, V. H. 2001 On the use of ultrasonics in hydrodynamic cavitation control. In *4th Intl Symp. on Cavitation, CAV2001, Caltech, Pasadena, California, USA* (ed. C. E. Brennen). California Institute of Technology.

Crum, L. A. 1975 Bjerknes forces on bubbles in a stationary sound field. *J. Acoust. Soc. Am.* **57**, 1369–1370.

Crum, L. A. 1984 Rectified diffusion. *Ultrasonics* **22**, 215–223.

Flynn, H. G. 1964 Physics of acoustic cavitation in liquids. In *Physical Acoustics: Principles and Methods* (ed. W. F. Mason), vol. 1B, pp. 58–172. Academic.

Flynn, H. G. & Church, C. C. 1984 A mechanism for the generation of cavitation maxima by pulsed ultrasound. *J. Acoust. Soc. Am.* **76**, 505–512.

Flynn, H. G. & Church, C. C. 1988 Transient pulsations of small gas bubbles in water. *J. Acoust. Soc. Am.* **84**, 985–998.

Fyrillas, M. M. & Szeri, A. 1994 Dissolution or growth of soluble spherical oscillating bubbles. *J. Fluid Mech.* **277**, 381–407.

Heuter, T. F. & Bolt, R. H. 1955 *Sonics*. John Wiley.

Kodama, Y., Tamiya, S., Take, N. & Kato, H. 1979 The effect of nuclei on the inception of bubble and sheet cavitation on axisymmetric bodies. In *ASME Intl Symp. on Cavitation Inception, New York* (ed. W. M. B. Morgan & B. R. Parkin), pp. 75–86.

Leighton, T. G. 1995 Bubble population phenomena in acoustic cavitation. *Ultrasonics Sonochemistry* **2** (2), s123–s126.

Moholkar, V. S. & Pandit, A. B. 2001 Numerical investigations in the behavior of one dimensional bubbly flow in hydrodynamic cavitation. *Chem. Engng Sci.* **56**, 1411–1418.

Oldenziel, D. M. 1982 A new instrument in cavitation research: the cavitation susceptibility meters. *Trans. ASME: J. Fluids Engng* **104**, 136–142.

Parlitz, U., Mettin, R., Luther, S., Akhatov, I., Voss, M. & Lauterborn, W. 1999 Spatio-temporal dynamics of acoustic cavitation bubble clouds. *Phil. Trans. R. Soc. Lond.* A **357**, 313–334.

Prosperetti, A. & Hao, Y. 1999 Modelling of spherical gas bubble oscillations and sonoluminescence. *Phil. Trans. R. Soc. Lond.* A **357**, 203–223.